

Optimizing Photovoltaic Performance by Kinetic Quenching of Layered Heterojunctions

Li-Feng Xu, Zhan-Wen Xu*, Jia-Ping Lin*, and Li-Quan Wang*

Shanghai Key Laboratory of Advanced Polymeric Materials, Key Laboratory for Ultrafine Materials of Ministry of Education, School of Materials Science and Engineering, East China University of Science and Technology, Shanghai 200237, China

 Electronic Supplementary Information

Abstract The mixing morphology control plays a crucial role in photovoltaic power generation, yet this specific effect on device performances remains elusive. Here, we employed computational approaches to delineate the photovoltaic properties of layered heterojunction polymer solar cells with tunable mixing morphologies. One-step quench and two-step quench strategies were proposed to adjust the mixing morphology by thermodynamic and kinetic effects. The computation for the one-step quench revealed that modulating interfacial widths and interfacial roughness could significantly promote the photovoltaic performance of layered heterojunction polymer solar cells. The two-step quench can provide a buffer at a lower temperature before the kinetic quenching, leading to the formation of small-length-scale islands connected to the interface and a further increase in photovoltaic performance. Our discoveries are supported by recent experimental evidence and are anticipated to guide the design of photovoltaic materials with optimal performance.

Keywords Dissipative particle dynamics; Drift-diffusion model; Polymer solar cells; Quench

Citation: Xu, L. F.; Xu, Z. W.; Lin, J. P.; Wang, L. Q. Optimizing photovoltaic performance by kinetic quenching of layered heterojunctions. *Chinese J. Polym. Sci.* 2022, 40, 29–37.

INTRODUCTION

Polymer solar cells (PSCs) are a kind of potential clean-energy technology, which holds promise for manufacturing lightweight and highly flexible devices such as portable electronic products and building-integrated photovoltaics.^[1–5] Although the power conversion efficiency was dramatically improved recently, it has not yet broken through the requirements of commercial markets due to the limitation on the mechanism of charge carrier generation and transport.^[6,7] To date, a considerable effort has been devoted to creating novel π -conjugated polymers to improve photovoltaic performance. In contrast, understanding the morphology effect on PSC performance and formulating basic rules that guide morphology optimization need to be further enhanced.

Optimizing the morphology is indispensable for the successful preparation of PSCs with outstanding performance.^[8–12] The PSC performance can be quantitatively correlated with phase purity and Flory-Huggins parameters.^[13] Insufficient phase separation in PSCs can lead to performance deteriorations. However, a larger repulsion between donors

and acceptors can lead to over-purification of mixed domains and decreased PSC performance.^[14] For example, Ade *et al.* observed that the average power conversion efficiency shows a substantial drop as the composition of the amorphous mixed domains is below the percolation threshold.^[15] Ye *et al.* recently found that such a problem can be resolved by kinetically quenching the mixed domains to an optimal composition close to the percolation threshold.^[16] Despite this, fundamental guidelines are still required to optimize PSC performances with optimal mixing morphologies. Combining thermodynamic effects and kinetic controls can assist the design of heterojunctions with varied mixing morphologies.^[16] The thermodynamics can drive the phase separation of donors and acceptors in PSCs, and the quench by kinetic control can "lock-in" instantaneous phase-separated morphologies. Recent attention has been paid to the stability of such mixing morphologies.^[17–20] However, little is known about the kinetic route to control mixing morphologies and the influence of mixing morphologies on PSC performances. Quantifying the impact of mixing morphology on device performance by developing kinetic control rules is the key to optimizing the heterojunction structure and promoting power conversion efficiency.

Theoretical computation and simulation, such as kinetic Monte Carlo simulations, can avoid trial-and-error experiments and improve experimental efficiency. The drift-diffusion model, requiring less computational cost than the kinet-

* Corresponding authors, E-mail: zhanwenxu@fudan.edu.cn (Z.W.X.)

E-mail: jlin@ecust.edu.cn (J.P.L.)

E-mail: lq_wang@ecust.edu.cn (L.Q.W.)

Received July 23, 2021; Accepted August 20, 2021; Published online November 9, 2021

ic Monte Carlo model, can predict the photovoltaic performances.^[21,22] Ganesan *et al.* predicted the photovoltaic performance of rod-coil block copolymers by inputting the density profile and orientational order parameter obtained from self-consistent field theory calculations into the drift-diffusion model.^[23] The drift-diffusion formalism allows them to account for spatially varying morphologies and the anisotropy in charge transport within an internally consistent framework. Dissipative particle dynamics (DPD), coupled with the drift-diffusion model, is an alternative to study the PSC performances.^[24–26] We have applied the DPD simulation to study the phase behavior of various polymer systems and used the drift-diffusion formalism to calculate the photovoltaic performance of block copolymer solar cells.^[24,25] The computation showed that the DPD coupled with a drift-diffusion model is a powerful tool for predicting performance and peering into the internal mechanism.

In this work, we conducted an *in silico* layer inter-diffusion experiment in the framework of DPD simulations. One-step and two-step quench strategies, based on thermodynamic driving and kinetic controlling, were proposed to regulate the mixing morphologies. The density information obtained from the DPD simulation was input to the drift-diffusion model to predict the photovoltaic properties. One-step quenching results demonstrated that optimal interfacial width results in the excellent photovoltaic performance of layered heterojunction. We discovered that the two-step quench could help to form rough interfaces and small-length-scale islanded structures connected with the interfaces, which are conducive to the improvement of photovoltaic performance. Our prediction shows good agreement with experimental findings and can explain the impact of PSC morphology on performances quantitatively.

COMPUTATIONAL METHODS

We developed a multiscale method combining dissipative particle dynamics (DPD) with a drift-diffusion model to investigate the PSC photovoltaic performance. The DPD was first conducted to obtain the structure of polymer blends consisting of donors (**D**) and acceptors (**A**). And then, the structures were input into the drift-diffusion model to calculate the photovoltaic performance. The DPD method and drift-diffusion model are given as follows.

DPD Method

The DPD, firstly proposed by Hoogerbrugge and Koelman, is a stochastic simulation technique for simulating the dynamic and rheological properties of complex fluids.^[27] The details of the DPD method can be found in Section 1 in the electronic supplementary information (ESI). A DPD bead represents a cluster of atoms/molecules in the method.^[28–33] The motion of DPD beads obeys the Newton equation of motion. The force applied to each bead comprises non-bonding forces and bonding forces. The non-bonding force \mathbf{f}_α applied on the α^{th} bead includes a conservative force $\mathbf{F}_{\alpha\beta}^C$, a dissipative force $\mathbf{F}_{\alpha\beta}^D$ and a random force $\mathbf{F}_{\alpha\beta}^R$. The neighboring beads in each polymer are connected by a harmonic spring potential $E_{\alpha\beta} = k_b(r_{\alpha\beta} - r_{\text{eq}})^2$ with the spring constant $k_b=100$ and the

equilibrium bond length $r_{\text{eq}}=0.86r_c$. All physical quantities are in reduced units, where the units of time, length, mass, and energy are τ , r_c , m , and $k_B T$, respectively. The physical lengths in our system were established as follows. We equated r_c to 2 nm to build a bridge between simulation parameters and experimental values. The thickness of layers sandwiched between two electrodes ($L_{\text{thickness}}$) was set to 100 nm, and the width L_{width} of each **A** (or **D**) layer is 20 nm.

We conducted the DPD simulations in a box with periodic boundary conditions. The NVT ensembles were adopted in the simulation, and the time step was set as $\Delta t=0.002\tau$. Considering the finite size effect, we chose the **A** (or **D**) polymer with six DPD beads, the size of which should be much smaller than the box size. The number of **A** (or **D**) polymers is 2000 to ensure that the number density of DPD beads is $3r_c^{-3}$. To simulate a layer inter-diffusion experiment, we arranged the **D** and **A** layers periodically with the lamellae perpendicular to the electrode (see the inset of Fig. 1a).^[13] The interaction strengths between the same kind of DPD beads are $a_{AA}=a_{DD}=25$. In the beginning, the simulation with $a_{DA}=100$ was performed for 1.0×10^4 DPD steps to relax the polymers in each layer and minimize the interface of mixed **D/A** polymers. The layered heterojunction model was prepared for subsequent kinetic quenching simulation. Then, the interaction strength is reduced to $a_{DA}=25$ to allow the inter-diffusion of the polymers. After t_1 , the simulation was stopped to mimic a one-step in-depth quenching process, and the simulation structures were taken as the one-step quenching structures. The mixed morphology can exhibit various states when we adopted different processing methods. In the two-step quench simulation, the interaction strength a_{DA} was increased after the simulation for t_1 , and then another simulation was performed for t_2 , as illustrated in Fig. 1(a). The varied interaction strengths a_{DA} correspond to various blending temperatures.

Drift-diffusion Model

We calculated the photovoltaic performances of PSCs with various structures by solving drift-diffusion equations.^[34,35] The details of the drift-diffusion model are provided in Section 2 in ESI. We solved the drift-diffusion equations numerically by finite difference methods. The equations are first discretized in three dimensions and then solved by the double conjugate gradient method and Gauss-Seidel iteration method. The parameters of the model used in the photovoltaic calculation are listed in Table S1 (in ESI). Most of the parameters are typical for polymeric materials used in PSCs.^[23–25,36] In solving drift-diffusion equations, the periodic boundary conditions were applied in the *x*- and *y*-directions parallel to electrodes. In contrast, the non-periodic boundary conditions in the *z*-direction normal to electrodes were set (for details, see Section 2 in ESI).

RESULTS AND DISCUSSION

The present work focuses on building the relationship between the mixing morphology and photovoltaic performances of polymer solar cells (PSCs). We considered a PSC system consisting of two kinds of homopolymers, that is, donor (**D**) polymers and acceptor (**A**) polymers, and used a multiscale

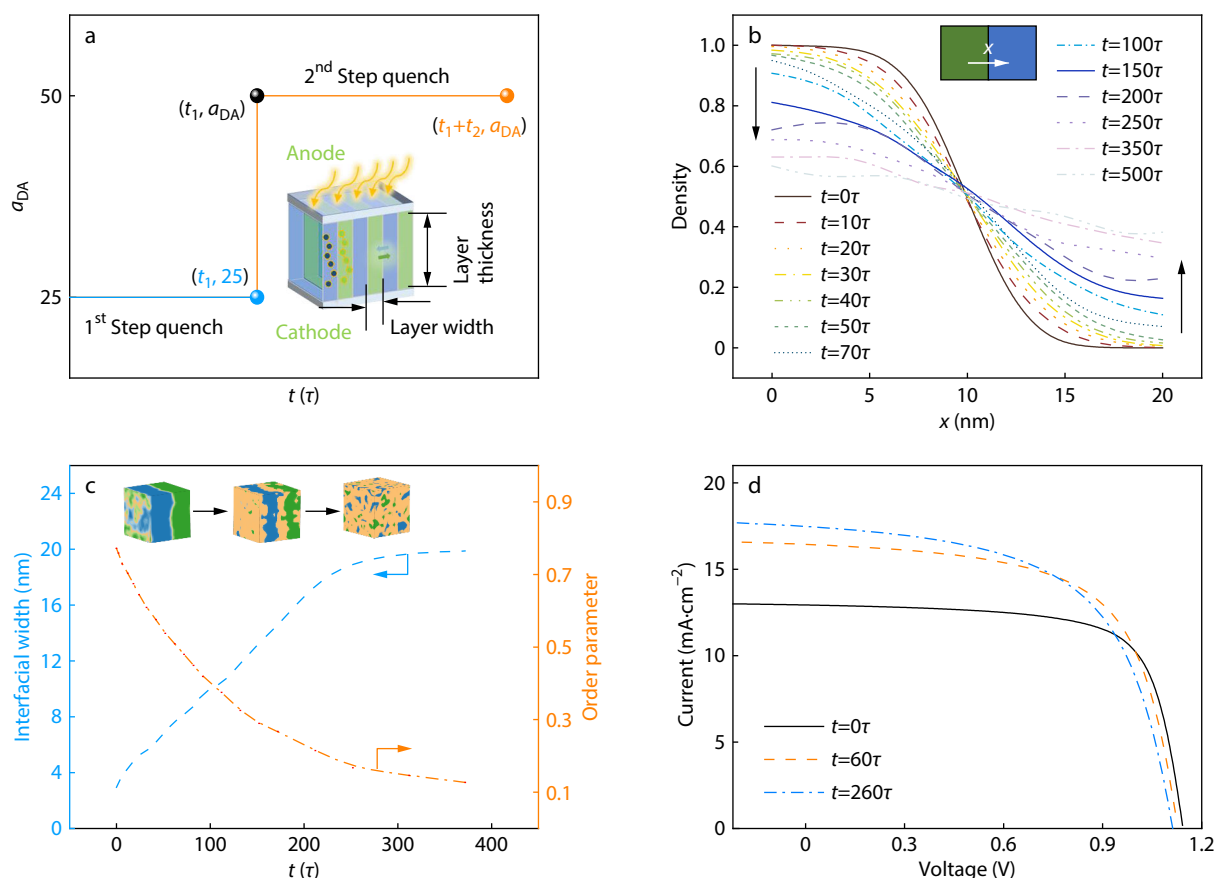


Fig. 1 (a) Schematic of the simulation method for one-step quenching and two-step quenching processes. In one-step quenching, $a_{DA}=25$, $t=t_1$, and $t_2=0$. In a representative two-step quench, the a_{DA} is 25 and 50 before and after t_1 , respectively. The inset shows the initial simulation model of PSC device, where the layer thickness and the layer width are 100 and 20 nm, respectively; (b) One-dimensional density profiles of acceptors along the x -direction normal to the interface at various blending time; (c) Plots of interfacial width and order parameter as a function of blending time t . The insets show the corresponding mixing morphologies, where blue, green, and brown colors are assigned to the **D** domain, the **A** domain, and the interface, respectively; (d) Plots of output current as a function of applied voltage for the layered heterojunction obtained at various blending time in a one-step quench.

method coupling DPD with drift-diffusion models to explore the morphology effect on PSC photovoltaic performances.^[24,25] The in silico experiment of layer inter-diffusion was first performed using DPD simulations, and then the photovoltaic performance of the PSC system was investigated by solving drift-diffusion equations.

To simulate a layer inter-diffusion experiment,^[13] we arranged the **D** and **A** layers periodically with the lamellae perpendicular to the electrode (Fig. 1a). We simulated both the one-step quench and two-step quench processes to obtain layered heterojunctions with varied mixing morphologies. In a one-step quench simulation, the blending time is continuously adjusted to gain layered heterojunction with various interfacial widths. In a two-step quench simulation, we can achieve the layered heterojunction with sufficient phase-separated mixed domains. The details can be found in the Computational Methods section.

One-step Quench

This subsection adopted a one-step quench method to achieve heterojunction structures with various interfacial widths and explored the relation between photovoltaic performances and interfacial width. In the initial period of quenching simulation,

the interaction strength a_{DA} between **D** and **A** polymers was set as 25, which equals the interaction strengths between the beads of the same type, to simulate the inter-diffusion of **D** and **A** polymers at high temperature. As time goes on, the **D/A** interface gradually widens through inter-diffusion, and the layered heterojunction slowly evolves toward a thoroughly mixing state (mixing heterojunction). To generate layered heterojunctions with various interfacial widths, we stopped the simulation at different time to mimic the quenching process where the temperature drops rapidly to freeze the movement of polymer chains. For example, melts of polymer blends are frozen into a glass below the glass transition temperature. The time when we stopped the simulation is referred to as blending time.

Fig. 1(b) shows the density profiles of **A** polymers obtained at various blending time. As shown, the fraction of **A** polymers in the acceptor-rich domain decreases as the blending time increases. As a result, the degree of mixing increases, and the **D/A** interface broadens. To qualify such a variation, we calculated the order parameter and interfacial width at various blending time (the definitions of order parameter and interfacial width are given in section 4 in ESI). The result is

shown in Fig. 1(c), where the orange and blue lines correspond to the order parameter and the interfacial width, respectively. As the blending time increases, the interfacial width shows a nearly linear increase and then keeps unchanged. Different from the interfacial width, the order parameter gradually decreases. This result implies that the variation of order parameters can be inversely related to the change of interfacial width. A plot of order parameters as a function of interfacial width proves such a relationship (Fig. S1 in ESI). Therefore, we only examined the effect of the interfacial width on photovoltaic performances in the following. We also found the **D** and **A** polymers are almost uniformly mixed (mixing heterojunction) at a long blending time (e.g., 370 τ).

The J - V curves were calculated for the layered heterojunctions obtained at various blending time, under applied voltages from -0.45 V to 1.3 V, using the drift-diffusion model. As the blending time increases, the short-current density (J_{SC}) increases, and the open-circuit voltages (V_{OC}) decrease (Fig. 1d). The output power first increases and then decreases as the applied voltage increases (Fig. S2 in ESI). The layered heterojunction generated at the blending time of 60 τ possesses the most superior maximum output power among the photovoltaic devices obtained at three blending times. The photovoltaic performances, including J_{SC} , V_{OC} , fill factor (FF), and power conversion efficiency (η), can be calculated from the J - V curves to characterize photovoltaic devices. Since the variation of mixing degrees can be related to the change of

interfacial widths (Fig. S1 in ESI), we focused on the dependence of performances on the interfacial width. Fig. 2 shows the variation of J_{SC} , V_{OC} , FF and η as a function of the interfacial width. As shown, the photovoltaic performances exhibit different responses to the change in interfacial width. The J_{SC} increases markedly with increasing the interfacial width, followed by a slight variation of the J_{SC} (Fig. 2a). Compared with J_{SC} , the values of V_{OC} are less sensitive to the variation of interfacial width (Fig. 2b). And the FF shows a decrease with increasing interfacial width, which resulted from the enhanced recombination of charge carriers (Fig. 2c). The η first increases and then decreases as the interfacial width increases (Fig. 2d). The optimal interfacial width is ca. 7 nm for the **D/A** heterojunction photovoltaic device. At optimal conditions, the corresponding order parameter is 0.54 (Fig. S1 in ESI). As the interfacial width is smaller than 7 nm, the charge carrier generation dominates the charge carrier recombination. In contrast, the charge carrier recombination governs the photovoltaic efficiency as the interfacial width becomes large.

To capture the underlying mechanism enhancing the photovoltaic performance of the layered heterojunction with intermediate interfacial width, we calculated two-dimensional distributions of acceptor volume fraction, exciton density, charge carrier generation rate, and charge carrier recombination rate. The two-dimensional distribution was obtained by projecting the three-dimensional distribution of acceptor volume fraction, exciton density X (m^{-3}), charge carrier generation rate G_{eh} ($\text{m}^{-3}\cdot\text{s}^{-1}$), and charge carrier recombination rate

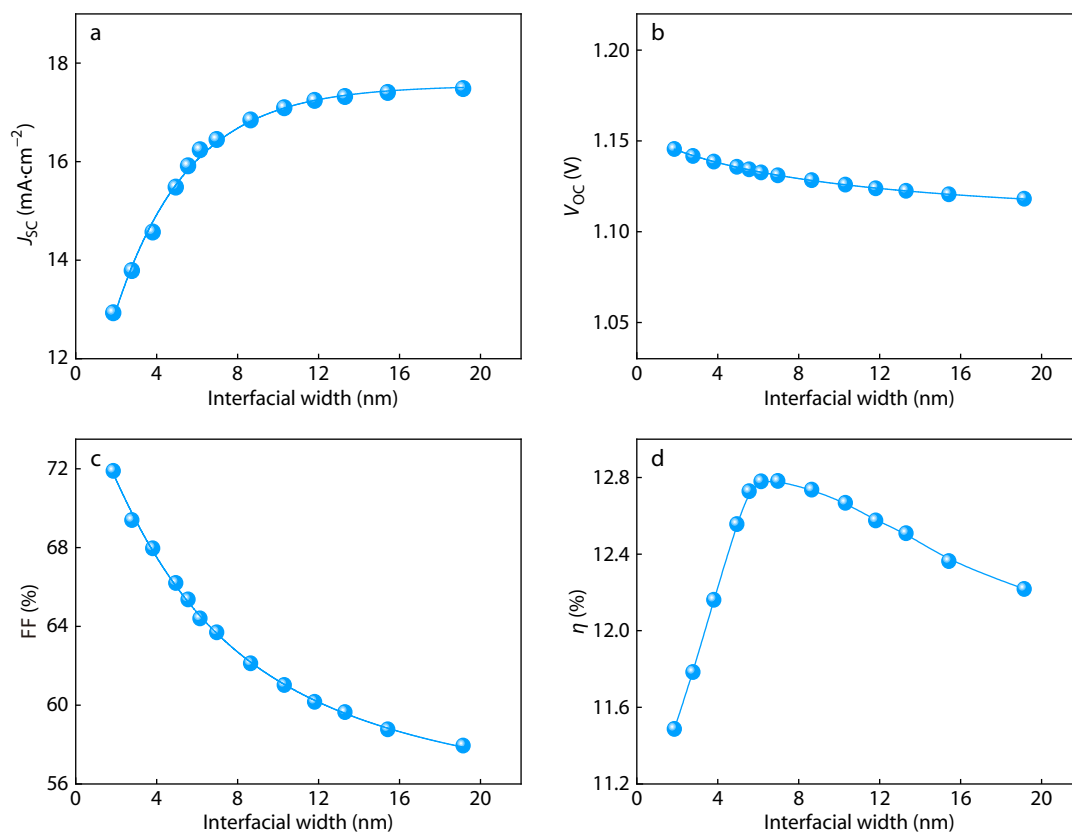


Fig. 2 Plots of (a) J_{SC} , (b) V_{OC} , (c) FF, and (d) η as a function of the interfacial width of heterojunction PSCs in a one-step quench. The width of each layer is 20 nm, and the interaction strength a_{DA} between **D** and **A** polymers is 25.

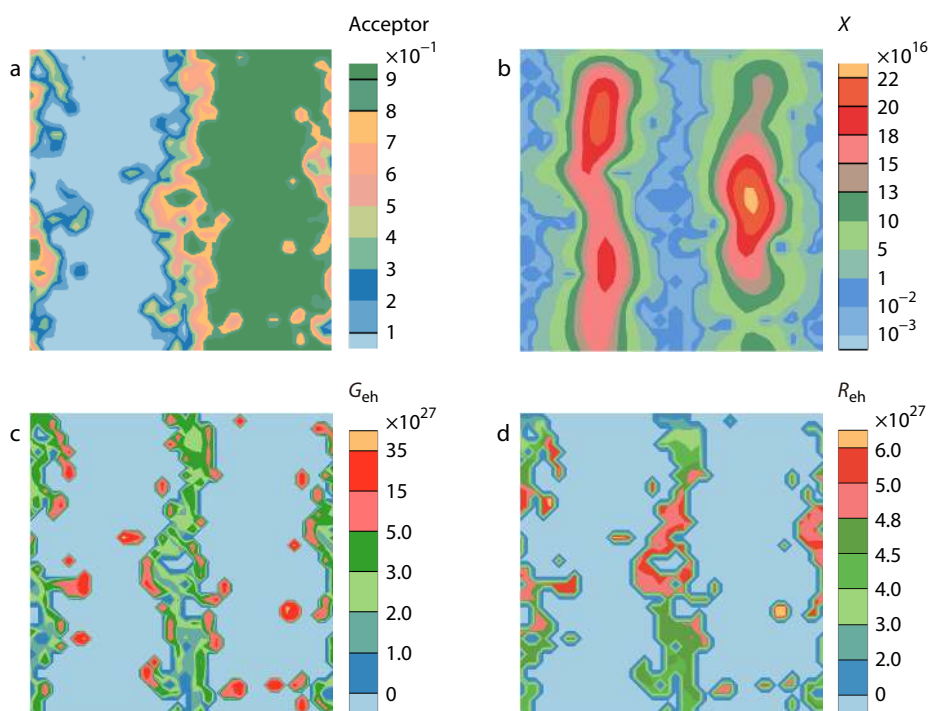


Fig. 3 Two-dimensional distributions of (a) acceptor volume fraction, (b) exciton density (m^{-3}), (c) charge carrier generation rate ($\text{m}^{-3}\cdot\text{s}^{-1}$), and (d) charge carrier recombination rate ($\text{m}^{-3}\cdot\text{s}^{-1}$) along x - and z -coordinates. The layered heterojunction has an interfacial width of 7 nm.

R_{eh} ($\text{m}^{-3}\cdot\text{s}^{-1}$) on the x - z plane because their distributions on the y -axis are reproducible. The results presented in Fig. 3 are for the polymer blends with an interfacial width of 7 nm. As shown in Fig. 3(a), the interface between **D** and **A** polymers is rough, which results in a substantial increase in the specific interface area of the heterojunction compared to planar heterojunction. The concentration of excitons near the interface drops significantly compared with those in the relative pure domain (Fig. 3b), which indicates the separation of a large number of excitons at the **D/A** heterojunction interface. Based on Figs. 3(c) and 3(d), we can intuitively observe the distribution of generation rate G_{eh} of charge carriers and recombination rate R_{eh} of charge carriers, where larger values near the interface and smaller values in the pure domain appear. One can see that the generation rate G_{eh} of charge carriers at the interface is higher than that inside the interface (Fig. 3c). The interface offers a central site for separating excitons and recombining charge carriers. Compared with the interface, the relative pure domain is a better channel for carrier transport in the photogeneration process for less doping of electrons or holes. The tradeoff between charge carrier generation and charge carrier recombination determines the optimal interfacial width. In addition, the interfacial roughness enables a portion of separated carriers to transport through pure domain channels, further increasing the performance.

The photovoltaic performances are dependent on the interaction strength a_{DA} and layer width L_{width} . As the layer width increases, the J_{SC} decreases, but the V_{OC} and FF increase (Figs. S3a–S3c in ESI). In addition, the optimal η decreases with the increases of layer width (Fig. S3d in ESI). The increase of layer width reduces the specific interfacial area for exciton separation, leading to the reduced η . As the layer

width increases, it requires more blending time to obtain the optimized specific interfacial area through inter-diffusion. As a consequence, the optimal η shifts to a long blending time as the layer width increases. The photovoltaic performance at the longer blending time shows no evident difference because the **A** and **D** polymers are homogeneously mixed ($a_{\text{DA}}=25$).

The interaction strength a_{DA} can be associated with the blending temperatures in the one-step quench experiment. Higher interaction strength means a lower blending temperature. The J_{SC} decreases, and the V_{OC} and FF increase as the a_{DA} increases (Figs. S4a–S4c in ESI). At the high a_{DA} value, e.g., $a_{\text{DA}}=32.5$, the photovoltaic performances are nearly unchanged, which results from deteriorative compatibility between the **D** and **A** polymers. The temporal variation of η depends much on the a_{DA} value (Fig. S4d in ESI). As the a_{DA} is not very high, the η changes non-monotonically with time, increasing first and then decreasing until it keeps unchanged. The optimal η increases and shifts towards long blending time with improving the a_{DA} . As the a_{DA} is high, e.g., at $a_{\text{DA}}=30$, the η varies monotonically with blending time—the η increases first and then stays nearly unchanged. Note that the mixing heterojunction and layered heterojunction are obtained at high and low blending temperatures, respectively, as the blend reaches equilibrium. At a low temperature, the η for the equilibrium structures obtained at long blending time decreases with increasing a_{DA} values, which could be ascribed to the interface narrowing in layered heterojunctions at a higher interaction strength.

Two-step Quench

In this subsection, we further optimized the layered heterojunction PSCs by secondary phase separation of mixing

domains. A two-step quenching process was proposed to modulate the phase separation and, therefore, the photovoltaic performance (Fig. 1b). In the two-step quenching process, the blending time t includes a high-temperature mixing time t_1 and a low-temperature separating time t_2 . At a time shorter than t_1 , the a_{DA} is 25, allowing **D** and **A** polymers to mix via interdiffusion at a high temperature. This process is the same as in the one-step quenching process. At a time longer than t_1 , the a_{DA} increases to 50 to drive microphase separation between **D** and **A** polymers. This case mimics the phase separation of polymer blends at a low temperature (still in the molten state). At the time of t_1+t_2 , we stopped the simulation to mimic an in-depth quenching process, where the temperature is decreased to, for example, below glass transition temperature to freeze polymer chains. Taking the one-step quenching process as the benchmark, we explored the effect of secondary phase separation on photovoltaic performances.

In the two-step quenching, the blending time t varies to

obtain morphologies with various separation/mixing degrees. We then calculated the photovoltaic performance of these layered heterojunctions under different blending time t . The result is presented in Fig. 4(a). The photovoltaic performance curve from 0 to t_1 is represented by a solid blue line, which shows no difference from the performance curve of the one-step quench. The dashed black curve represents the photovoltaic performance curve from t_1 to t_1+t_2 . For each t_1 (blue dot), we selected the optimal photovoltaic efficiency η^* at the second-step quench and represented it with an orange dot. We connected the orange dots into a curve to represent optimal photovoltaic efficiency curves after two-step quenching treatment under various conditions. As the t increases, the optimal photovoltaic efficiency increases initially and then decreases slowly, whose trend is similar to that of a one-step quenching process. With increasing t_1 , the time t_2 required to achieve the optimal photovoltaic efficiency η^* increases, especially in the late stage ($t_1 > 70\tau$). The result im-

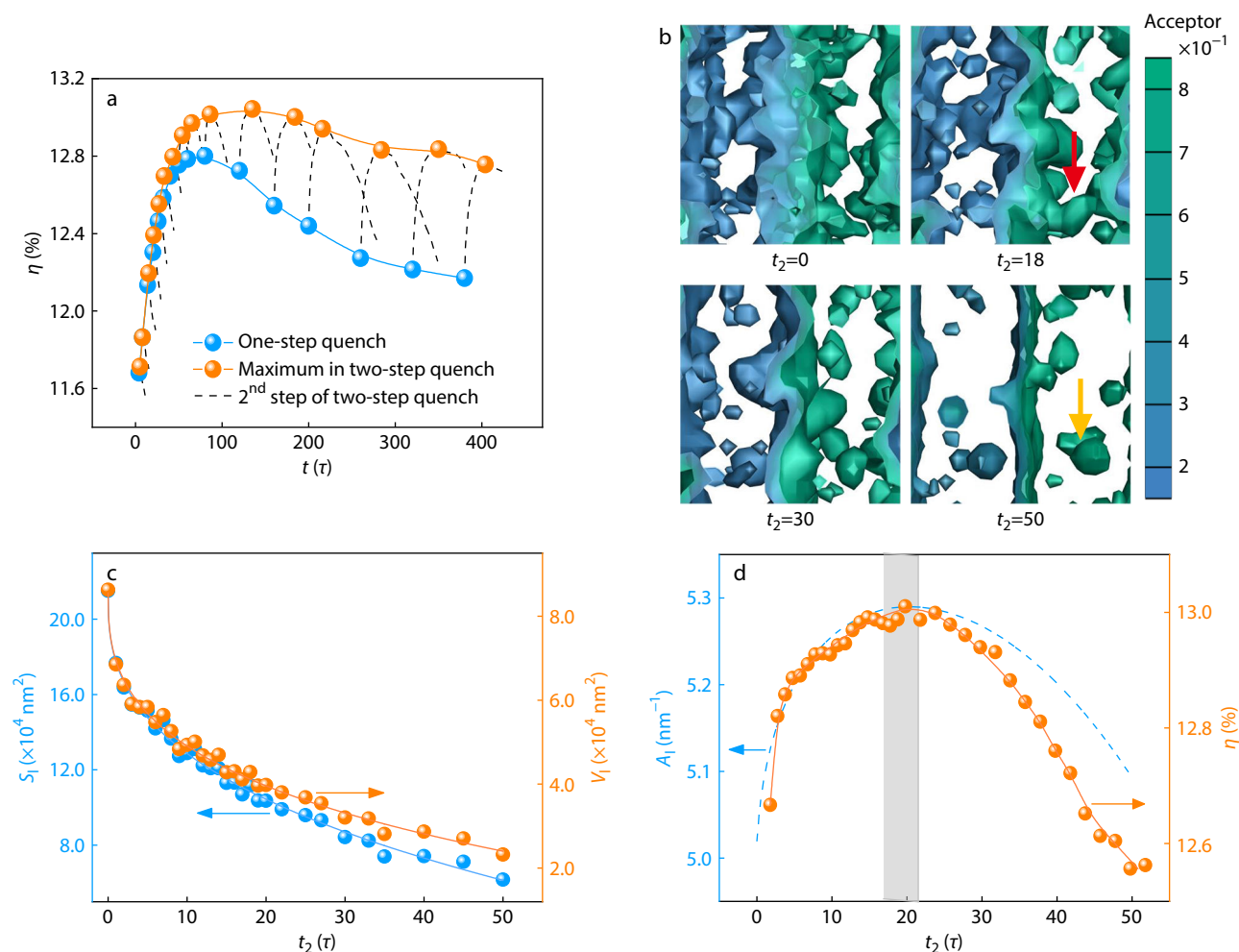


Fig. 4 (a) Plots of η as a function of time t for the two-step quenching process, in which high-temperature mixing time t_1 and low-temperature phase separating time t_2 are adjusted continuously. The solid blue curve and dashed black lines refer to the first-step and second-step quenching processes, respectively. (b) Front view of the layered heterojunction obtained at $t_2 = 0, 18, 30$, and 50 , respectively, where the high-temperature mixing time $t_1 = 120\tau$. The red and yellow arrows indicate the island connected to the interface and isolated island, respectively. (c) Plots of volume V and interfacial area S of the heterojunction as a function of the low-temperature phase separating time t_2 . (d) Plots of specific interfacial area A deduced from $S(t_2)/V(t_2)$ and photovoltaic performances as a function of low-temperature phase separating time t_2 . The high-temperature mixing time t_1 is 120τ .

plies that the two-step quenching treatment contributes much to the performance enhancement. Compared with the best photovoltaic performance of 12.78% in the one-quench process, the two-step quenching treatment can improve the device to higher photovoltaic performance, *ca.* 13.05% at $t_1=120\tau$ and $t_2=18\tau$.

We found that the interaction strength has a less marked effect on the optimal photovoltaic efficiency as the interaction strength is higher, for example, at $a_{DA}=40, 50,$ and 60 (Fig. S5 in ESI). The low-temperature phase-separating time t_2 required to achieve optimal photovoltaic efficiency decreases for each case as the interaction strength increases. However, as the interaction strength is lower, *e.g.*, at $a_{DA}=30$, the optimal photovoltaic efficiency shows an evident difference from those of higher interaction strengths. A much longer phase-separating time t_2 is required to achieve optimal photovoltaic efficiency.

The improved photovoltaic performance can be related to the secondary phase separation between donor and acceptor polymers in the mixing domains. Fig. S6 (in ESI) shows the order parameter as a function of separating time t_2 . As shown, the order parameter increases with time, and the donor and acceptor polymers become more phase-separated. The optimized performance was obtained at an intermediate order parameter of 0.64, implying that either insufficient phase separation or the over-purification of the acceptor- or donor-rich domains can lead to performance deteriorations. Since the phase separation can occur both at the interface and within **A**- and **D**-rich domains, the mechanism behind the performance optimization needs to be explored further.

To obtain a deep insight into the internal mechanism underlying the enhanced photovoltaic performances at $t_2=18\tau$, we captured the morphologies of the **D/A** heterojunction at various low-temperature separating time t_2 . The results are shown in Fig. 4(b). As shown, as t_2 increases from 0τ to 18τ , the interfacial region gradually narrows, indicating the phase separation. Moreover, the phase separations within **D** and **A**-rich domains also happen, leading to a series of small-length-scale islanded structures. At that time, the **D/A** interface is highly structured and rough, and the phase-separated small-length-scale islands are connected with the interface to form continuous structures. Such an arrangement results in increased interfaces for exciton separation and efficient passages for charge transport. Therefore, the η reaches the highest value. As t_2 further increases, the phase separation goes on, and the interface becomes less structured and narrow, leading to a decreased exciton separation efficiency. At $t_2=50\tau$, a flat, thin interface appears between **D**- and **A**-rich domains. Moreover, the small-length-scale islands are independent of the interface and become "isolated islands" within **D**- or **A**-rich domains, resulting in the loss of effective transport channels. The less structured interface, narrow interfacial width, and isolated small-length-scale islands are harmful to the exciton separation, leading to decreased power conversion efficiency. The two-step quench provides a buffer for making the interface rough and generating small-length-scale islands connected to the interface at a lower temperature before the kinetic quenching, leading to improved performance.

To further quantify the impact of interfacial roughness on device performance, we analyzed the morphology features of the **D/A** heterojunction by Minkowski functionals V and S at $t_1=120\tau$. As shown in Fig. 4(c), with t_2 increasing from 0τ to 50τ , the volume V and interfacial area S of the heterojunction present the same tendency to go down faster at first and then decrease slower. In this process, the acceptor and donor polymers tend to come together, and the purity of the acceptor- or donor-rich domain increases. We obtained the curves of specific interfacial area A_l with time t_2 from $S(t_2)/V(t_2)$, which is shown in Fig. 4(d). The curves of the specific interfacial area of the heterojunction and the photovoltaic performance show similar trends, both of which increase initially and reach a peak in the dash region (t_2 is around 18τ), and then drop off. The result implies that an increase in specific interfacial areas is a critical factor for improving photovoltaic performance. The low-temperature phase separation in the two-step quench plays a role in modulating the specific interfacial area.

Comparison with Existing Experimental Observations

There is some experimental evidence available to support the simulation results. Ye *et al.* recently carried out a bilayer inter-diffusion experiment to gain insight into the relationship between interaction parameters and photovoltaic performances of organic solar cells.^[13] They established a quantitative "constant-kink-saturation" relation between Flory-Huggins parameter χ_{DA} and the fill factor FF in organic solar cells. To make a comparison, we calculated the FF for the equilibrium **D/A** blends obtained at various interaction strengths a_{DA} through one-step quench simulations for a long bending time.

Fig. 5 shows the plot of fill factors as a function of Flory-Huggins parameter χ_{DA} between donor and acceptor. The χ_{DA} is related to a_{DA} in terms of $\chi_{DA} = (0.286 \pm 0.02) \Delta a$.^[37] In the figure, the blue and orange dots correspond to the experimental and simulation results, respectively. Similar to the experimental findings, the simulation also revealed a "constant-kink-saturation" relation between FF and χ_{DA} ; that is, as the χ_{DA} increases, the FF is first almost unchanged, then increases sharply, and finally keeps nearly unchanged (Fig. 5). However, the FF in the simulation is higher than that in experiments.

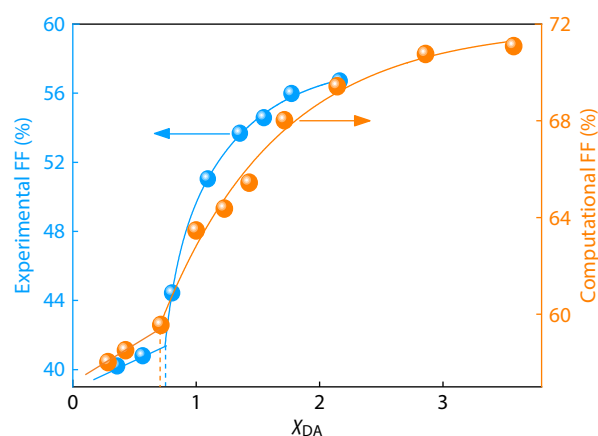


Fig. 5 Plots of fill factor FF as a function of Flory-Huggins parameter χ_{DA} for layered heterojunctions obtained in a one-step quench. The experimental results (blue dots) were adapted from Ref. [13] with the permission of Nature Publishing Group.

This difference could result from the discrepancy between the experimental sample and the simulation model. Different from the all-polymer system in simulation, the experimental model adopts the PCDTBT:PC₇₁BM system. The molecule acceptor phases diffuse into donor phases faster, and the donor region has a lower purity, which results in the rise of carrier recombination. The donor composition in the acceptor-rich domains is unequal to the acceptor composition in the donor-rich domains in the experiment. However, in our simulation, the acceptor-rich and donor-rich domains are symmetric, and both of them can contribute to the FF, resulting in an increased FF. Despite that, the "constant-kink-saturation" features are consistent. We found that a sharp increase in FF happens as χ_{DA} is higher than *ca.* 0.75. This threshold value, associated with the phase separation between donors and acceptors, is similar to that (*ca.* 0.72) revealed in the experiment. The consistency with experimental results implies that the current simulation is a practical approach to reproducing the experimental observations.

Recently, Ade *et al.* observed a substantial drop in power conversion efficiency as the mixed domain is over-purified.^[15] Reducing the interaction strength between acceptors and donors can avoid the over-purification of the domains. However, higher interaction strength is still needed for phase separation and, thus, optimal performance. Therefore, there is a need to kinetically quench the mixed domains to a composition close to the percolation threshold for achieving optimal performance if the molecular interaction of constituent materials is too repulsive. Ye *et al.* recently determined the quench depth of an organic solar cell to achieve optimal performance and stabilize the mixing morphology.^[16,38] The essence of their work is to create percolation structures with continuous channels by a kinetic quench. In our simulation, we found that the connectivity of islanded structures in **D/A** domains with the interface is crucial to the performance enhancement (Fig. 4b). The formation of islands can increase the interface, whereas the connectivity with the interface can offer transport channels. Such an observation is consistent with the opinion that sufficient electron pathways for transport are a critical morphological requisite for achieving desirable PSC performances, although the length scale we focused on is much smaller than that of mixed domains in the experiments.

Similar to polymer blends, block copolymers can also yield various ordered morphologies. Provided that the interfacial width and domain size of the lamellae formed by block copolymers are similar to those of mixing morphology, the photovoltaic properties could be the same. We can expect the variation of photovoltaic properties by changing the interface width and domain size *via* varying the chemistry of blocks and the length of block copolymers. Changing the chemical species and polymer lengths requires synthesizing new polymers, which usually poses challenges. In contrast, the mixing morphology can be readily obtained by kinetically quenching the polymer blends, although the quench system is generally more unstable than the block copolymer system. Overall, the block copolymers can achieve similar photovoltaic performance with polymer blends, but their morphologies are regulated through different routes.

In this work, we discovered that appropriately modulating

interfacial width, interfacial roughness, and islands' connectivity with interfaces can enhance photovoltaic performance. We proposed two quenching methods to adjust these structures of the layered heterojunctions. The work revealed that a specific buffer time for blending and secondary phase separation could increase the interfacial area and form electron transport pathways, leading to enhanced photovoltaic performance. Recent observations demonstrated that quenching to the percolation threshold is critical to performance improvement.^[16,38] Our work adds a new opinion to the current findings: providing a buffer at a lower temperature before the kinetic quenching can further increase photovoltaic performance.

CONCLUSIONS

The DPD method, coupled with the drift-diffusion model, was employed to study the mixing morphology effect on the photovoltaic performance of layered heterojunction PSCs. We performed an *in silico* layer inter-diffusion experiment and designed two quench approaches to regulating the mixing morphology of layered heterojunctions, that is, one-step quench and two-step quench. In the one-step quench, the layered heterojunction with intermediate interfacial width exhibits an optimal photovoltaic performance. We further enhanced the power conversion efficiency of the layered heterojunction by modulating the mixing morphology with a two-step quench method. We discovered that the interfacial width, interfacial roughness, and small-length-scale island structures formed within acceptor- and donor-rich domains combinedly affect the power conversion efficiency. Our work delineates the effect of quenching processes on photovoltaic performance, which could be beneficial to the design and quantitative optimization of active layers.

NOTES

The authors declare no competing financial interest.



Electronic Supplementary Information

Electronic supplementary information (ESI) is available free of charge in the online version of this article at <https://doi.org/10.1007/s10118-021-2642-8>.

ACKNOWLEDGMENTS

This work was financially supported by the National Natural Science Foundation of China (Nos. 21774032, 51833003 and 51621002).

REFERENCES

- 1 Chu, S.; Majumdar, A. Opportunities and challenges for a sustainable energy future. *Nature* **2012**, *488*, 294–303.
- 2 Creutzig, F.; Agoston, P.; Goldschmidt, J. C.; Luderer, G.; Nemet, G.; Pietzcker, R. C. The underestimated potential of solar energy to mitigate climate change. *Nat. Energy* **2017**, *2*, 17140.
- 3 Song, S.; Lee, K. T.; Koh, C. W.; Shin, H.; Gao, M.; Woo, H. Y.; Vak, D.;

- Kim, J. Y. Hot slot die coating for additive-free fabrication of high performance roll-to-roll processed polymer solar cells. *Energy Environ. Sci.* **2018**, *11*, 3248–3255.
- 4 Chiang, Y. F.; Jeng, J. Y.; Lee, M. H.; Peng, S. R.; Chen, P.; Guo, T. F.; Wen, T. C.; Hsu, Y. J.; Hsu, C. M. High voltage and efficient bilayer heterojunction solar cells based on an organic-inorganic hybrid perovskite absorber with a low-cost flexible substrate. *Phys. Chem. Chem. Phys.* **2014**, *16*, 6033–6040.
 - 5 Li, K.; Zhen, H.; Niu, L.; Fang, X.; Zhang, Y.; Guo, R.; Yu, Y.; Yan, F.; Li, H.; Zheng, Z. Full-solution processed flexible organic solar cells using low-cost printable copper electrodes. *Adv. Mater.* **2014**, *26*, 7271–7278.
 - 6 Zhang, J.; Zhu, L.; Wei, Z. Toward over 15% power conversion efficiency for organic solar cells: current status and perspectives. *Small Methods* **2017**, *1*, 1700258.
 - 7 Mukherjee, S.; Jiao, X.; Ade, H. Charge creation and recombination in multi-length scale polymer:fullerene BHJ solar cell morphologies. *Adv. Energy Mater.* **2016**, *6*, 1600699.
 - 8 Huang, Y. C.; Tsao, C. S.; Huang, T. Y.; Cha, H. C.; Patra, D.; Su, C. J.; Jeng, U. S.; Ho, K. C.; Wei, K. H.; Chu, C. W. Quantitative characterization and mechanism of formation of multilength-scale bulk heterojunction structures in highly efficient solution-processed small-molecule organic solar cells. *J. Phys. Chem. C* **2015**, *119*, 16507–16517.
 - 9 Zhuo, Z. L.; Zhang, F. J.; Xu, X. W.; Wang, J.; Lu, L. F.; Xu, Z. Photovoltaic performance improvement of P3HT:PCBM polymer solar cells by annealing treatment. *Acta Phys.-Chim. Sin.* **2011**, *27*, 875–880.
 - 10 Liu, Y.; Zhao, J.; Li, Z.; Mu, C.; Ma, W.; Hu, H.; Jiang, K.; Lin, H.; Ade, H.; Yan, H. Aggregation and morphology control enables multiple cases of high-efficiency polymer solar cells. *Nat. Commun.* **2014**, *5*, 5293.
 - 11 Liao, H. C.; Ho, C. C.; Chang, C. Y.; Jao, M. H.; Darling, S. B.; Su, W. F. Additives for morphology control in high-efficiency organic solar cells. *Mater. Today* **2013**, *16*, 326–336.
 - 12 Yao, H.; Ye, L.; Hou, J.; Jang, B.; Han, G.; Cui, Y.; Su, G. M.; Wang, C.; Gao, B.; Yu, R.; Zhang, H.; Yi, Y.; Woo, H. Y.; Ade, H.; Hou, J. Achieving highly efficient nonfullerene organic solar cells with improved intermolecular interaction and open-circuit voltage. *Adv. Mater.* **2017**, *29*, 1700254.
 - 13 Ye, L.; Hu, H.; Ghasemi, M.; Wang, T.; Collins, B. A.; Kim, J. H.; Jiang, K.; Carpenter, J. H.; Li, H.; Li, Z.; McAfee, T.; Zhao, J.; Chen, X.; Lai, J. L. Y.; Ma, T.; Bredas, J. L.; Yan, H.; Ade, H. Quantitative relations between interaction parameter, miscibility and function in organic solar cells. *Nat. Mater.* **2018**, *17*, 253–260.
 - 14 Ghasemi M.; Hu H.; Peng Z.; Rech, J. J.; Angunawela, I.; Carpenter, J. H.; Stuard, S. J.; Wadsworth, A.; McCulloch, I.; You, W.; Ade, H. Delineation of thermodynamic and kinetic factors that control stability in non-fullerene organic solar cells. *Joule* **2019**, *3*, 1328–1348.
 - 15 Bartelt, J. A.; Beiley, Z. M.; Hoke, E. T.; Mateker, W. R.; Douglas, J. D.; Collins, B. A.; Tumbleston, J. R.; Graham, K. R.; Amassian, A.; Ade, H.; Frechet, J. M. J.; Toney, M. F.; McGehee, M. D. The importance of fullerene percolation in the mixed regions of polymer-fullerene bulk heterojunction solar cells. *Adv. Energy Mater.* **2013**, *3*, 364–374.
 - 16 Ye, L.; Li, S.; Liu, X.; Zhang, S.; Ghasemi, M.; Xiong, Y.; Hou, J.; Ade, H. Quenching to the percolation threshold in organic solar cells. *Joule* **2019**, *3*, 443–458.
 - 17 Tada, A.; Geng, Y.; Wei, Q.; Hashimoto, K.; Tajima, K. Tailoring organic heterojunction interfaces in bilayer polymer photovoltaic devices. *Nat. Mater.* **2011**, *10*, 450–455.
 - 18 Nam, Y. M.; Huh, J.; Jo, W. H. Optimization of thickness and morphology of active layer for high performance of bulk-heterojunction organic solar cells. *Sol. Energy Mater. Sol. Cells* **2010**, *94*, 1118–1124.
 - 19 Huang, J. H.; Li, K. C.; Kekuda, D.; Padhy, H. H.; Lin, H. C.; Ho, K. C.; Chu, C. W. Efficient bilayer polymer solar cells possessing planar mixed-heterojunction structures. *J. Mater. Chem.* **2010**, *20*, 3295–3300.
 - 20 Dennler, G.; Scharber, M. C.; Brabec, C. J. Polymer-fullerene bulk-heterojunction solar cells. *Adv. Mater.* **2009**, *21*, 1323–1338.
 - 21 Groves, C. J. E.; Science, E. Developing understanding of organic photovoltaic devices: kinetic monte carlo models of geminate and non-geminate recombination, charge transport and charge extraction. *Energy Environ. Sci.* **2013**, *6*, 3202–3217.
 - 22 Bartesaghi, D.; van der Kaap, N.; Koster, L. J. A. 3D simulations of organic solar cells. In *Unconventional thin film photovoltaics*, RSC Publishing, **2016**; pp 420–452.
 - 23 Shah, M.; Ganesan, V. Correlations between morphologies and photovoltaic properties of rod-coil block copolymers. *Macromolecules* **2010**, *43*, 543–552.
 - 24 Xu, Z.; Lin, J.; Zhang, L.; Wang, L.; Wang, G.; Tian, X.; Jiang, T. Distinct photovoltaic performance of hierarchical nanostructures self-assembled from multiblock copolymers. *ACS Appl. Mater. Interfaces* **2018**, *10*, 22552–22561.
 - 25 Xu, Z.; Lin, J.; Zhang, L.; Tian X.; Wang, L. Modulation of molecular orientation enabling high photovoltaic performance of block copolymer nanostructures. *Mater. Chem. Front.* **2019**, *3*, 2627–2636.
 - 26 Du, C.; Ji, Y.; Xue, J.; Hou, T.; Tang, J.; Lee, S. T.; Li, Y. Morphology and performance of polymer solar cell characterized by DPD simulation and graph theory. *Sci. Rep.* **2015**, *5*, 16854.
 - 27 Hoogerbrugge, P. J.; Koelman, J. M. V. A. Simulating microscopic hydrodynamic phenomena with dissipative particle dynamics. *Europhys. Lett.* **1992**, *19*, 155–60.
 - 28 Wang, L.; Ma, J.; Hong, W.; Zhang, H.; Lin, J. Nanoscale diffusion of polymer-grafted nanoparticles in entangled polymer melts. *Macromolecules* **2020**, *53*, 8393–8399.
 - 29 Hong, W.; Lin, J.; Tian, X.; Wang, L. Distinct viscoelasticity of hierarchical nanostructures self-assembled from multiblock copolymers. *Macromolecules* **2020**, *53*, 10955–10963.
 - 30 Hong, W.; Lin, J.; Tian, X.; Wang, L. Viscoelasticity of nanosheet-filled polymer composites: three regimes in the enhancement of moduli. *J. Phys. Chem. B* **2020**, *124*, 6437–6447.
 - 31 Romyantsev, A. M.; Gavrilov, A. A.; Kramarenko, Y. E. Electrostatically stabilized microphase separation in blends of oppositely charged polyelectrolytes. *Macromolecules* **2019**, *52*, 7167–7147.
 - 32 Santo, K. P.; Vishnyakov, A.; Kumar, R.; Neimark, A. V. Elucidating the effects of metal complexation on morphological and rheological properties of polymer solutions by a dissipative particle dynamics model. *Macromolecules* **2018**, *51*, 4987–5000.
 - 33 Chakraborty, S.; Choudhury, C. K.; Roy, S. Morphology and dynamics of carbon nanotube in polycarbonate carbon nanotube composite from dissipative particle dynamics simulation. *Macromolecules* **2013**, *46*, 3631–3638.
 - 34 Buxton, G. A.; Clarke, N. Computer simulation of polymer solar cells. *Model. Simul. Mater. Sci.* **2007**, *15*, 13–26.
 - 35 Barker, J. A.; Ramsdale, C. M.; Greenham, N. C. Modeling the current-voltage characteristics of bilayer polymer photovoltaic devices. *Phys. Rev. B* **2003**, *67*, 075205.
 - 36 Ray, B.; Alam, M. A. Random vs regularized OPV: limits of performance gain of organic bulk heterojunction solar cells by morphology engineering. *Sol. Energy Mater. Sol. Cells* **2012**, *99*, 204–212.
 - 37 Groot, R. D.; Warren, P. B. Dissipative particle dynamics: bridging the gap between atomistic and mesoscopic simulation. *J. Chem. Phys.* **1997**, *107*, 4423–4435.
 - 38 Ghasemi, M.; Balar, N.; Peng, Z.; Hu, H.; Qin, Y.; Kim, T.; Rech, J. J.; Bidwell, M.; Mask, W.; McCulloch, I.; You, W.; Amassian, A.; Risko, C.; O'Connor, B. T.; Ade, H. A molecular interaction-diffusion framework for predicting organic solar cell stability. *Nat. Mater.* **2021**, *20*, 525–532.